ADVANCED HEALTHCARE MATERIALS
www.advhealthmat.de

Photopolymerizable Hydrogel for Enhanced Intramyocardial Vascular Progenitor Cell Delivery and Post-Myocardial Infarction Healing

Xuechong Hong, Allen Chilun Luo, Ilias Doulamis, Nicholas Oh, Gwang-Bum Im, Chun-Yen Lin, Pedro J. del Nido, Ruei-Zeng Lin, and Juan M. Melero-Martin**

Cell transplantation success for myocardial infarction (MI) treatment is often hindered by low engraftment due to washout effects during myocardial contraction. A clinically viable biomaterial that enhances cell retention can optimize intramyocardial cell delivery. In this study, a therapeutic cell delivery method is developed for MI treatment utilizing a photocrosslinkable gelatin methacryloyl (GelMA) hydrogel. Human vascular progenitor cells, capable of forming functional vasculatures upon transplantation, are combined with an in situ photopolymerization approach and injected into the infarcted zones of mouse hearts. This strategy substantially improves acute cell retention and promotes long-term post-MI cardiac healing, including stabilized cardiac functions, preserved viable myocardium, and reduced cardiac fibrosis. Additionally, engrafted vascular cells polarize recruited bone marrow-derived neutrophils toward a non-inflammatory phenotype via transforming growth factor beta (TGFβ) signaling, fostering a pro-regenerative microenvironment. Neutrophil depletion negates the therapeutic benefits generated by cell delivery in ischemic hearts, highlighting the essential role of non-inflammatory, pro-regenerative neutrophils in cardiac remodeling. In conclusion, this GelMA hydrogel-based intramyocardial vascular cell delivery approach holds promise for enhancing the treatment of acute myocardial infarction.

1. Introduction

Myocardial infarction (MI) remains a significant global health concern.[1,2] MI's progression involves the rapid onset of ischemia-induced myocardial necrosis, leading to the replacement of the infarct zone by fibrotic tissues.[3] Despite advances in surgical interventions, pharmacotherapy, and mechanical devices reducing acute mortality,[4] these strategies provide only modest, long-term improvements in cardiac function.[5,6] As a result, many patients eventually develop complications such as heart failure and arrhythmia.[2] Therapeutic approaches focusing on the delivery of genes, growth factors, and cells have shown promise in promoting MI healing.[7–11] However, the complex hyper-inflammatory microenvironment within the infarcted myocardium has limited effectiveness.[12–16]

Preclinical studies have demonstrated promise for cell-based therapies in mitigating ventricular remodeling and enhancing MI recovery.[1,2] These therapies typically involve the transplantation of patches derived from pluripotent stem cells[17] or the direct injection of therapeutic cells into infarcted areas.[18] Minimally invasive surgical techniques allow for early cell delivery during the acute MI phase,[9] and a variety of adult stem/progenitor cells, including cardiosphere-derived cells,[19] bone marrow-derived mononuclear cells,[20,21] endothelial progenitor cells,[22] and mesenchymal stem cells (MSCs),[23] are under exploration. Interestingly, paracrine factors from non-myocyte cell types seem to contribute beneficially to cardiac remodeling and the modulation of the inflammatory response.[7,12,23] However,

X. Hong, A. C. Luo, I. Doulamis, N. Oh, G.-B. Im, P. J. del Nido, R.-Z. Lin, J. M. Melero-Martin
Department of Cardiac Surgery
Boston Children's Hospital
Boston, MA 02115, USA
E-mail: ruei-zeng.lin@childrens.harvard.edu; juan.meleromartin@childrens.harvard.edu

X. Hong, I. Doulamis, N. Oh, G.-B. Im, P. J. del Nido, R.-Z. Lin, J. M. Melero-Martin
Department of Surgery
Harvard Medical School
Boston, MA 02115, USA

J. M. Melero-Martin
Harvard Stem Cell Institute
Harvard University
Cambridge, MA 02138, USA

C.-Y. Lin
Department of Lymphoma and Myeloma
The University of Texas
M. D. Anderson Cancer Center
Houston, TX 77030, USA

The ORCID identification number(s) for the author(s) of this article can be found under https://doi.org/10.1002/adhm.202301581

DOI: 10.1002/adhm.202301581

the mechanisms underlying these effects are not yet fully understood.

Vascular progenitor cell delivery has emerged as a potentially promising therapeutic strategy for ischemic cardiomyopathy. Several studies have concentrated on delivering vascular cells to stimulate angiogenesis and construct new blood vessels.[24–26] This approach aims to rapidly reestablish microvascular networks within the ischemic myocardium, thus mitigating adverse remodeling. For example, in a rat model of myocardial ischemia/reperfusion injury (IRI), human endothelial colony-forming cells (ECFCs) and MSCs injected in phosphate-buffered saline (PBS) demonstrated a modest decrease in adverse ventricular remodeling.[24] However, quantitative analysis revealed a swift loss of human cells post-myocardial injection, suggesting that inadequate cellular retention might be a significant factor in the muted therapeutic effect.[24] As such, the potential of human vascular progenitor cells with vasculogenic capabilities to mitigate adverse remodeling and promote functional recovery remains an open question.

Low cell retention and engraftment pose significant challenges to achieving substantial functional benefits in MI treatment, regardless of the cell type utilized.[27] The active motion of the beating heart often expels therapeutic cells injected in liquid vehicles, leading to an acute cell retention rate of only 0.5–10% in various studies encompassing different cell types, animal models, and delivery routes.[27–33] To address these challenges, various biomaterials aimed at enhancing cell engraftment have been explored. For example, Garcia et al. pioneered a gel injection technique that poses a reduced risk of embolization and thrombotic occlusion and introduced an innovative method for delivering hydrogels to the epicardium via the pericardial space.[34] Numerous studies have employed injectable hydrogels like N-isopropylacrylamide (NIPAM)-based Microgel,[35] self-assembling peptide in Puramatrix,[36] and NIPAM nanogel.[37] These studies reported outcomes such as diminished scar sizes and enhanced myocardial restoration post 28-day treatment, underscoring the potential of these biomaterials. Notably, the use of NIPAM nanogel in tandem with human cardiac stem cell transplantation resulted in the highest left ventricular ejection fraction (LVEF) at the 3-week mark.[37] However, the potential toxicity of the NIPAM monomer and the yet to be assessed host effects of Puramatrix peptides necessitate caution. Such studies underscore the significant progress and inherent challenges in leveraging biomaterials like GelMA for myocardial infarction treatment. While these materials have paved the way for improvements like increased cell retention and viability, the lasting impact of these therapies on cardiac functional metrics, both with and without cells, merits further study.

In this study, we employ gelatin methacryloyl (GelMA) hydrogel, a well-characterized material, for the delivery of human ECFCs and MSCs to foster neo-vascular networks in the ischemic myocardium. GelMA, a photocrosslinkable, bioadhesive hydrogel, polymerizes rapidly in myocardial tissues without compromising therapeutic cell viability.[38–40] We postulated that this rapid polymerization would prevent hydrogel dissemination at the implantation site. Additionally, we have previously shown that GelMA is fully compatible with ECFC-based vascular morphogenesis,[39] making it suitable for vascular cell therapy in infarcted hearts.

Our findings demonstrate that GelMA hydrogel can be transmyocardially photocrosslinked to maintain vascular cell retention in infarcted mouse hearts. This GelMA-assisted cell delivery approach facilitated infarct healing and adaptive remodeling, thus preserving cardiac function. Crucially, enhanced cell retention allowed for the first-time study of the early beneficial effects of human vascular cells in MI. Our data show that improved retention of human ECFCs and MSCs fostered perivascular-endothelial cell interactions, upregulating transforming growth factor beta (TGFβ) expression. TGFβ signaling encouraged the polarization of non-inflammatory, pro-regenerative neutrophils, which proved to be vital mediators of beneficial cardiac remodeling.

2. Results

2.1. In Situ Polymerization of GelMA Hydrogel Facilitates Cell Delivery in Infarcted Myocardium

We evaluated the in vivo application of transmyocardial polymerization of GelMA for cell delivery using a mouse model of MI (**Figure 1**). MI was induced in 10–12-week-old SCID mice by permanently ligating the left anterior descending (LAD) arteries (Figure S1A and Video S1, Supporting Information). A combination of human vascular progenitor cells (ECFCs and MSCs; 5×10^5 for each cell type) was suspended in 5% (w/v in PBS) GelMA precursor solution, and this mixture was promptly injected into the infarcted myocardium within 10 min of LAD ligation. The total injection volume per heart was 100 µL, which we confirmed to be sufficient to cover the infarct zone (Figure S1B, Supporting Information).

The complexity of directly measuring the total energy dosage of UV light led us to select the specific crosslinking condition of GelMA used. Specifically, we selected the crosslinking condition based on the minimum UV intensity needed to prevent the immediate leakage of the injected cells from mouse hearts. This decision was also informed by findings from our previous research, where we demonstrated that lower GelMA crosslinking/stiffness supports better blood vessel formation by the engrafted ECFCs and MSCs as well as facilitates the infiltration of supporting host myeloid cells into the graft.[39,40] We determined that UV light could permeate the myocardium of mice using our OmniCure S2000 UV lamp (wavelength 320–500 nm; intensity of 40 mW cm^{-2}), allowing GelMA polymerization within 10 s of transmyocardial UV exposure (Video S2, Supporting Information). The safety of this brief UV illumination method was established in a previous study,[40] confirming that our working range of UV light exposure (10–45 s) is benign to both the injected cells and surrounding tissues.[40]

2.2. GelMA Hydrogel Augments Cell Retention in Ischemic Hearts

We evaluated acute myocardial retention of human vascular progenitor cells by injecting 5×10^5 luciferase-labeled ECFCs (luc-ECFCs) with 5×10^5 non-labeled MSCs per heart and quantifying the bioluminescence intensity in the infarcted myocardium (Figure 1C). We compared the results of transmyocardial photocrosslinking of cell-laden GelMA hydrogel (GelMA-hydrogel

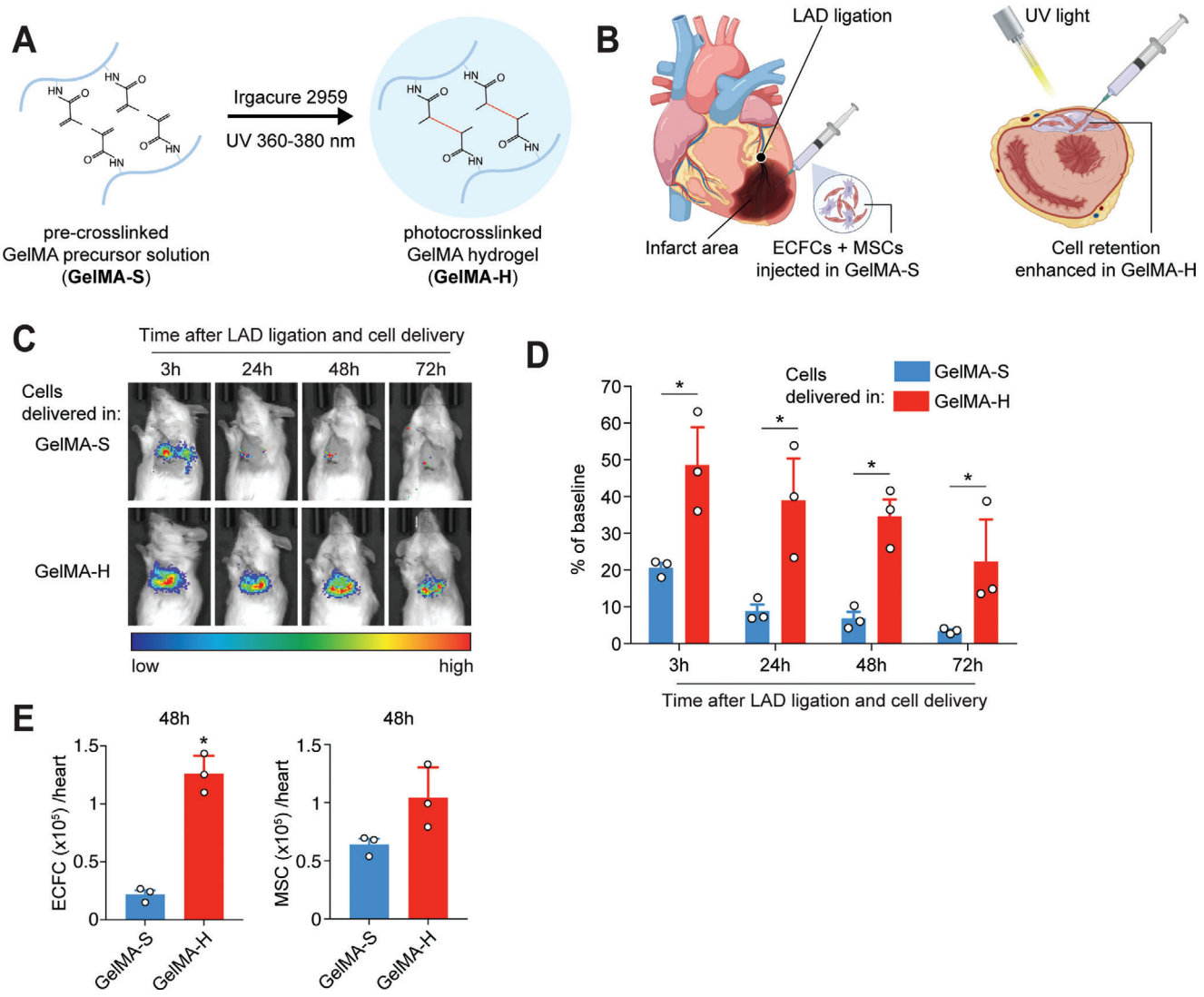

Figure 1. Enhanced intramyocardial retention of human vascular progenitor cells delivered in a photocrosslinked GelMA hydrogel. A) Schematic depicting the photocrosslinking of GelMA from a precursor solution (GelMA-S) to a hydrogel matrix (GelMA-H) under UV irradiation. B) Schematic depicting the intramyocardial cell injection. MI was surgically induced by LAD ligation. Human vascular progenitor cells (ECFCs + MSCs) resuspended in GelMA precursor solution were injected into three locations in the infarcted area. UV light was immediately applied on top of the infarcted area to polymerize the cell-laden hydrogel (referred to as GelMA-H group). UV irradiation was omitted for the control group to maintain cells injected in GelMA precursor solution (GelMA-S group). C) Viable cell retention was measured by bioluminescence imaging of human ECFCs expressing a luciferase reporter. D) Total bioluminescent signals in each animal's chest region were measured on 3, 24, 48, and 72 h post-MI and compared to the baseline (i.e., cells delivered to arrested mouse hearts). E) Retention of human ECFCs or MSCs was quantified by flow cytometric analysis on 48 h post-MI. Data correspond to cell numbers from each harvested MI heart. Data are mean ± s.d.; $n = 3$ mice per group (indicated by individual dots). $^*P < 0.05$ between GelMA-H and GelMA-S. Statistical methods: two-way ANOVA followed by Bonferroni's post-test analysis (D) and unpaired two-tailed Student's *t*-tests (E).

or GelMA-H group; Figure 1B) with cell injection in the same GelMA precursor solution but without UV illumination (GelMA-solution or GelMA-S group). Importantly, the GelMA precursor solution remains liquid under physiological conditions if not crosslinked by UV light.[41] To establish a baseline, we injected the same number of human cells into arrested mouse hearts and measured bioluminescence after 15 min (Figure 1D).

By the third hour after MI induction and cell delivery (3 h post-MI), ECFC presence in the GelMA-S group had decreased to 20.6 + 2.3% (Figure 1C,D), a retention rate similar to previous studies with intramyocardial cell delivery in PBS.[20,29,42] In contrast, the GelMA-H group showed a significant improvement in ECFC retention, with a rate of 48.6 ± 13.6% (3 h, $^*P < 0.05$ vs cells in GelMA-S; Figure 1D), confirming the potential of GelMA hydrogel in reducing cell backwash. This enhanced retention was sustained over a 3-day monitoring period post-MI (Figure 1D).

Flow cytometry results confirmed that GelMA-H improved the retention of both ECFCs and MSCs (Figure S2, Supporting Information, and Figure 1E; $P = 0.0005$ for ECFCs and 0.0728 for MSCs). The GelMA-H group preserved 25.2% of viable ECFCs and 20.8% of MSCs, compared to the GelMA-S group's retention of only 4.4% of ECFCs and 12.8% of MSCs.

Significantly, the GelMA hydrogel maintained the engraftment of ECFCs and MSCs close to the optimal 1:1 ratio required for long-term vascularization.[43] Overall, our findings suggest that rapid in situ photopolymerization of GelMA hydrogel effectively protects human vascular progenitor cells and reduces the acute phase "washout" effect post-MI.

2.3. GelMA Hydrogel-Delivered Human Vascular Progenitor Cells Enhance Cardiac Remodeling

We sought to understand whether the increase in acute cell retention would affect post-MI cardiac healing, assessing cardiac functions like left ventricular fractional shortening (LVFS) and LVEF through echocardiography (**Figure 2** and S3, Supporting Information). Baseline cardiac function, measured 1 hour before LAD ligation, showed no significant difference between groups. However, 7 days post-MI, both LVFS and LVEF were significantly higher in mice treated with human cells delivered in GelMA-H compared to untreated or GelMA-S-treated animals (Figure 2B,C). Post-treatment, both cardiac functions were substantially higher in the GelMA-H group and demonstrated significant improvement on days 7, 14, and 21 compared to the GelMA-S group.

The untreated and GelMA-S-treated groups exhibited a continuous decline in LVEF and LVFS from day 3 to 28 post-MI, indicating a deterioration of cardiac function due to adverse infarct remodeling. The lack of significant difference in LVEF and LVFS between untreated and GelMA-S-treated groups suggests negligible therapeutic benefit in low cell retention groups. Conversely, the GelMA-H group generally preserved cardiac function from day 3 to day 28.

Myocardium salvage after MI is a critical determinant for long-term preservation of cardiac function and survival.[2] We measured the myocardial wall thickness via echocardiography and found that the GelMA-H group displayed a significantly higher left ventricular anterior wall thickness (LVAW) than the untreated or GelMA-S groups (Figure 2D). Histological analysis further confirmed myocardium preservation in the GelMA-H group with a significant improvement in myocardial thickness compared to the untreated or GelMA-S groups after 4 weeks (Figure 2F; 0.44 + 0.05 mm versus 0.25 + 0.06 mm, $^{**}P < 0.05$). Masson's trichrome staining of 4-week harvested cardiac tissues also affirmed significantly reduced myocardial fibrosis in the GelMA-H group compared to the untreated or GelMA-S-treated groups (Figure 2G,H).

Taken together, our findings suggest that enhancing acute cell retention leads to beneficial cardiac remodeling, encompassing improved revascularization, decreased scar tissue formation, and stabilization of overall cardiac functions post-MI.

2.4. Formation of Functional Human Vasculature in Infarcted Hearts

We next explored the therapeutic mechanism resulting from the delivery of human vascular progenitor cells in GelMA-H. We examined the infarcted hearts on day 7 to evaluate the formation of human blood vessels.[24] Immunofluorescence staining for human-specific vimentin antibodies (staining both human ECFCs and MSCs) and UEA-I lectins (binding specifically to human ECFCs, not mouse endothelial cells) was used for histological examination. This revealed a significant difference in vascular network formation between the GelMA-H and GelMA-S groups (Figure 2I). The GelMA-H group demonstrated significant engraftment of human ECFCs and MSCs, as evidenced by the formation of human-specific vascular networks within the infarcted myocardium (Figure 2J,K). In contrast, the GelMA-S group displayed minimal engraftment of human MSCs in the infarcted myocardium, with no evidence of ECFC staining. These results suggest that in situ photocrosslinking of GelMA hydrogel significantly enhances the retention of co-delivered human ECFCs and MSCs. Without timely gelation of the GelMA hydrogel, even though some MSCs could engraft, ECFCs were unable to contribute to the revascularization of the infarcted myocardium.

The establishment of functional human vasculature in ischemic tissues could partially explain the therapeutic benefits observed in the GelMA-H group. However, we observed significant improvements in LVAW in the GelMA-H group as early as day 3 (Figure 2D), and improved cardiac functions by day 7 (LVFS and LVEF; Figure 2B,C). Given that human blood vessel perfusion begins ≈7 days after vascular progenitor cell implantation in this model,[39,40,44–46] this timing discrepancy between human cell-mediated revascularization and beneficial cardiac remodeling suggests that additional therapeutic pathways may be involved in preserving cardiac functions during the early stage of MI.

2.5. Gene Expression Analysis Following Human Vascular Progenitor Cell Delivery in Infarcted Hearts

To further understand the molecular underpinnings of the therapeutic benefits observed from the delivery of ECFC+MSC in GelMA-H, we performed an exploratory transcriptional analysis using bulk RNA sequencing (RNAseq). Infarcted left ventricle tissues were harvested from both GelMA-H and GelMA-S groups two days post-MI to examine changes in gene expression profiles at the early stages of treatment. Tissues from uninjured hearts served as controls.

At a global level, we detected differentially expressed genes (DEGs) among all three groups (Figure S4A, Supporting Information). Hierarchical clustering analysis (Figure S4B, Supporting Information) showed greater similarity between the two post-MI groups (GelMA-H and GelMA-S) compared to the uninjured controls. This pattern was also corroborated by principal component analysis (PCA; Figure S4C, Supporting Information). We then performed a gene ontology (GO) analysis on the DEGs between the post-MI GelMA-H group and the uninjured controls (Figure S4D, Supporting Information). The analysis revealed that the top enriched GO categories related to infarct injury and therapeutic cell delivery were primarily involved in the positive regulation of immune responses, such as inflammatory response, immune response, and leukocyte chemotaxis. This suggests that the immune system plays a significant role in the early stages of the MI process.

To gain more insight into the transcriptional differences between the GelMA-H and GelMA-S groups, we conducted a pairwise analysis of DEGs. We found 137 genes that were

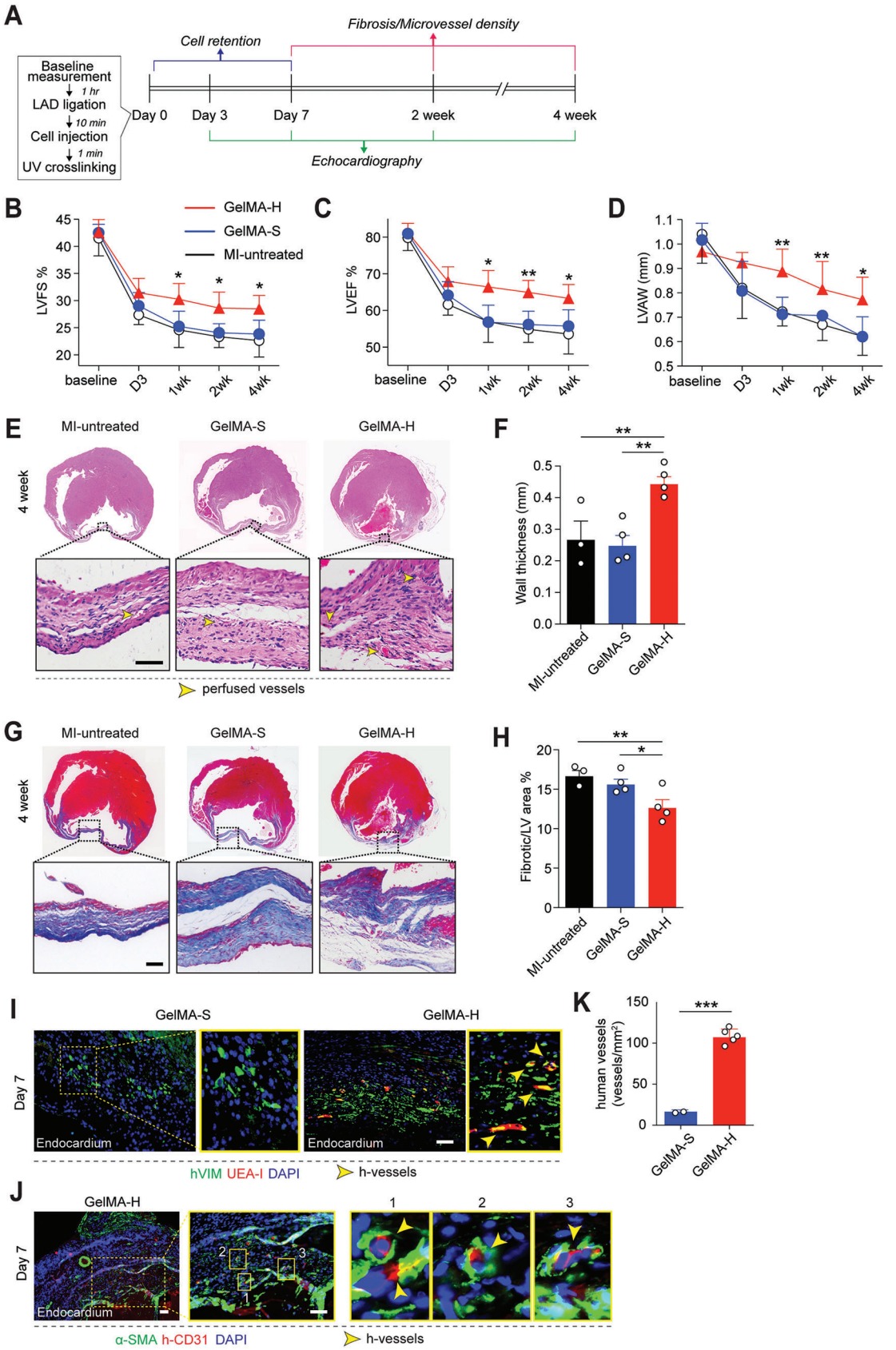

significantly upregulated in the GelMA-H group, whereas 617 genes were downregulated (Figure S4A, Supporting Information, GelMA-H vs GelMA-S). The volcano plot (Figure S4E, Supporting Information) displays the up- and down-regulated genes when comparing the GelMA-H group to the GelMA-S group. Notably, we observed upregulation of several genes related to neutrophil development and maturation in the GelMA-H group, such as *s100a8, s100a9, elane, ngp, mpo, camp, lef1,* and *ms4a2*. This was associated with the upregulation of genes involved in immature neutrophil trafficking (*sdf, cxcr4*) and hematopoiesis (*gata1, hemgn*) in the GelMA-H group compared to the GelMA-S group (Figure S4F,G, Supporting Information). Collectively, these data suggest a potential influence of human ECFCs and MSCs in GelMA-H on the recruitment and polarization of neutrophil subpopulations during the early stages of MI. However, it is important to note that there was significant data variation between samples within the GelMA-H group.

2.6. Recruitment of Neutrophils with Reparative Phenotype in GelMA-H Group

Our RNAseq data analysis indicated differences in neutrophil-related genes between the GelMA-H and GelMA-S groups. We previously demonstrated that human vascular progenitor cells implanted in vivo could polarize neutrophils toward a non-inflammatory phenotype, which mediates vascular assembly and anastomosis.[45] Recent studies have also shown that pro-regenerative neutrophils (termed here as NR; "R" for regeneration) play a role in coordinating tissue repair in various organs.[47–57] However, the role of NR in post-MI healing is not yet fully understood. Consequently, we chose to focus our studies on neutrophil polarization following MI.

We first examined early-stage host cell infiltration post-MI (**Figure 3**). On day 2, we analyzed by flow cytometry the recruited mouse CD45+ leukocytes in the infarcted myocardium, classifying them into Ly6G+F4/80- neutrophils or Ly6G-F4/80+ macrophages (Figure 3A). As expected in immunodeficient mice, the infiltration of Ly6G-F4/80- lymphocytes was negligible.[45] Also, the presence of resident murine myeloid cells in the uninjured myocardium was low (Figure 3B). LAD ligation followed by either GelMA-H or GelMA-S treatment significantly recruited host myeloid cells (Figure 3B), aligning with the induced innate immune response observed in the RNAseq analysis. Furthermore, the GelMA-H group recruited more neutrophils and macrophages than the GelMA-S group (Figure 3B), in line with our previous observation of host myeloid cell engagement by ECFCs and MSCs.[45] In contrast, the number of resident hematopoietic cells in uninjured hearts was relatively low (averaging 5.5×10^4 mCD45+ hematopoietic cells, 3.2×10^4 neutrophils, and 2×104 macrophages per uninjured heart).

We further evaluated neutrophil subpopulations using flow cytometry, classifying Ly6G+F4/80- cells into naïve neutrophils (N0; CXCR2-), pro-inflammatory neutrophils (NI; CXCR2+CD206-), and pro-regenerative neutrophils (NR; CXCR2+CD206+; Figure 3A,C). The NI subpopulation was dominant (83.27% of total neutrophils; Figure 3D) in MI mice treated with GelMA-S, consistent with previous reports showing pro-inflammatory neutrophils significantly mediating adverse cardiac remodeling in the first 7 days post-MI.[50] Conversely, NIs were considerably reduced (18.02%) in the GelMA-H group, where NRs were significantly more abundant (57.66% of total neutrophils), suggesting a shift toward NR polarization. The GelMA-H group also recruited more naïve neutrophils from the bone marrow than the GelMA-S group (24.32% vs 13.31%).

Altogether, these data suggest that improving human vascular progenitor cell retention could lead to a pro-regenerative host neutrophil polarization during the early stage of MI healing. Since NRs have been previously shown to promote tissue healing by facilitating the resolution of inflammation and stimulating angiogenesis, cell proliferation, and extracellular matrix (ECM) remodeling,[45,58–60] the increased abundance of NR in the GelMA-H group could partly explain the observed beneficial effects on cardiac function.

2.7. Human Vascular Cell Interaction Upregulated NR Polarization Factor TGFβ1

Next, we explored whether the prolonged retention and interaction between human ECFCs and MSCs in the GelMA-H group resulted in the release of paracrine factors that could promote NR polarization and whether these factors were absent in the GelMA-S group. For this purpose, we collected conditioned media from in vitro ECFCs + MSCs cocultures in GelMA hydrogel (CM^{CO}; **Figure 4**A). Subsequently, murine naïve neutrophils isolated from bone marrow (BM) were cultured in CM^{CO} for 24 h. NR polarization was indicated by the upregulation of *Il4, Vegfa,* and *Arg1* gene expressions upon exposure to CM^{CO} (Figure 4B). However, the evidence for NR polarization was minimal when BM neutrophils were cultured in basal medium or conditioned media obtained from ECFC or MSC monocultures (CM^{ECFC} or CM^{MSC}), suggesting an important role for ECFC-MSC crosstalk in NR polarization.

Figure 2. Human vascular progenitor cells delivered in GelMA hydrogel improved cardiac remodeling. A) Diagram of experimental schedule. B–D) Echocardiography analysis for cardiac function. Echocardiography was performed on anesthetized mice at 3 days and 1, 2, and 4 weeks post-MI following cell delivery in GelMA-H or GelMA-S ($n = 6$ for each group). Mice received LAD ligation, but no cell injection (MI-untreated) served as control ($n = 6$). Baseline data were obtained from mice within 1 h before performing LAD ligation. B) Left ventricular fractional shortening (LVFS). C) Left ventricular ejection fraction (LVEF). D) Left ventricular anterior wall thickness (LVAW). E) Representative heart horizontal panoramic views (upper) and microscopic images (lower) of myocardial sections stained with H&E at 4 weeks post-MI. Scale bars, 100 µm. F) The LV wall thickness in the infarcted areas quantified from H&E sections. G) Representative heart sections stained with Masson's trichrome at 4 weeks post-MI. Scale bars, 100 µm. H) The percentage of fibrotic areas in the total LV cross-sections quantified by Masson's trichrome staining. I,J) Histological analysis of the infarcted myocardium (the infarct and border zone regions) on day 7 revealed the presence of perfused human blood vessels only when cells were delivered in GelMA-H group, but not in GelMA-S. Human microvessels were identified by immunostaining for human-specific vimentin (hVIM) and UEA-I lectin binding (I) and human-specific CD31 (h-CD31) and α-SMA (J). Scale bars, 100 µm. K) Total perfused human microvessel density quantified in the infarcted myocardium. Statistical methods: ANOVA followed by Bonferroni's post-test analysis (B-D) and unpaired two-tailed Student's *t*-tests (F, H, J). Data present mean ± s.d. $^*P < 0.1$, $^{**}P < 0.05$, $^{***}P < 0.001$.

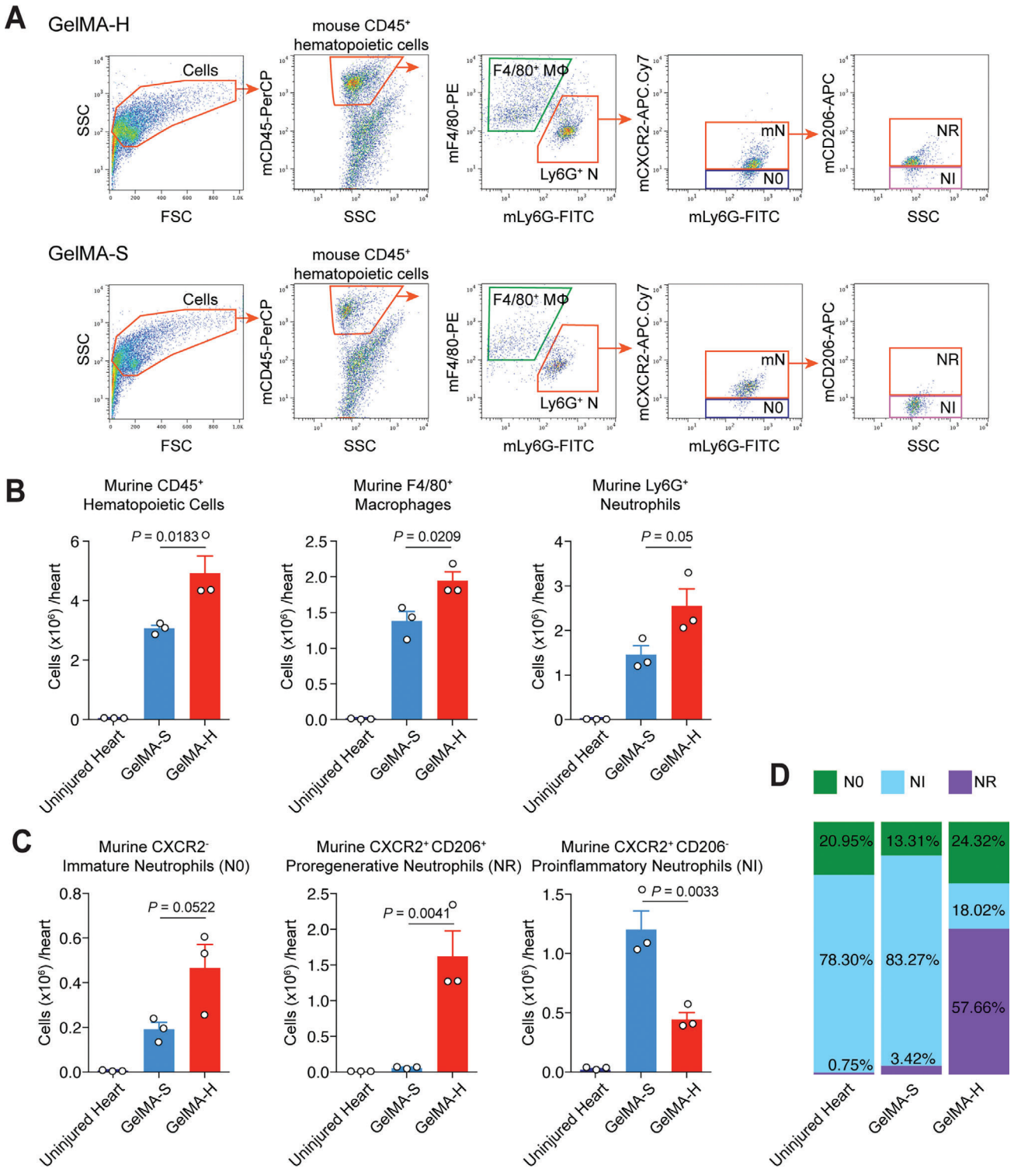

Figure 3. Human vascular progenitor cell retention promotes the recruitment of neutrophils with a reparative phenotype. The infarcted myocardial tissue was harvested on day 2 post-MI. Tissues were digested into single-cell suspensions for flow cytometric analysis. A) Flow cytometry gating strategy to identify recruited myeloid cells. Representative flow cytometric analyses of ischemic myocardium injected with ECFC + MSC in GelMA-S or GelMA-H. MΦ, macrophages; N, neutrophils; mN, mature neutrophils; N0, naïve neutrophils; NR, pro-regenerative neutrophils; NI, pro-inflammatory neutrophils. B) Quantitative cytometric analyses of murine CD45+ hematopoietic cells, Ly6G$^-$F4/80$^+$ macrophages, and total Ly6G$^+$F4/80$^-$ neutrophils obtained from the ischemic myocardium. The myocardium from uninjured hearts served as controls. C) Recruited Ly6G$^+$F4/80$^-$ neutrophils were classified into three subpopulations: N0 (CXCR2$^-$), NI (CXCR2$^+$CD206$^-$), and NR (CXCR2$^+$CD206$^+$). B,C) Data are mean ± s.d.; $n = 3$ per group; P values between GelMA-S and GelMA-H are listed. D) Proportions of the three neutrophil subpopulations in each group.

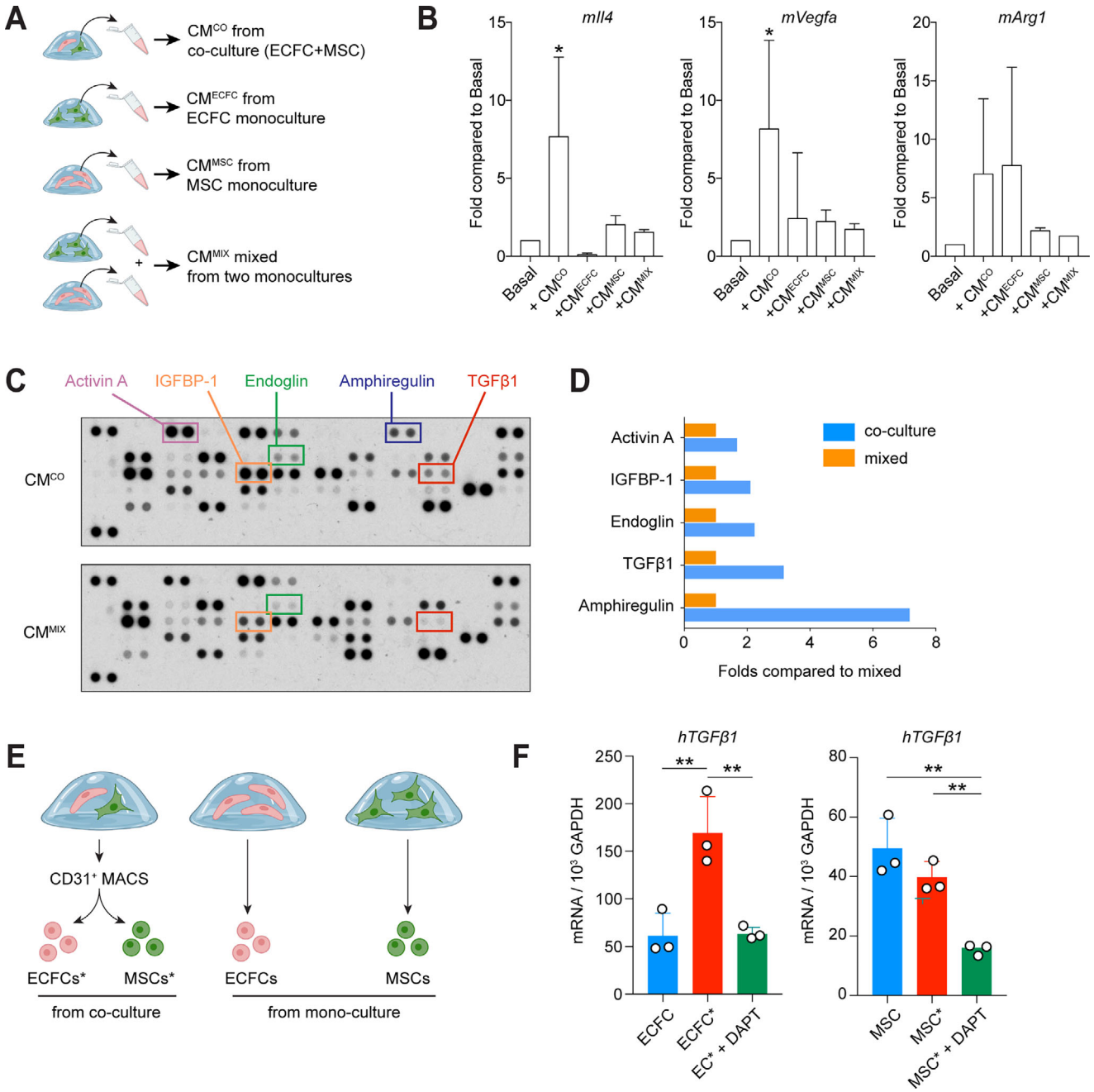

Figure 4. Human vascular progenitor cell crosstalk upregulates NR polarization factor TGFβ1. A) Conditioned media (CM) were collected from ECFC + MSC coculture in GelMA hydrogels in vitro (CM^{CO}). CMs obtained from ECFC or MSC monoculture (CM^{ECFC} or CM^{MSC}) and mixed in 1:1 ratio (termed CM^{MIX}) served as a control. B) Mouse naïve neutrophils isolated from bone marrow were cultured in basal medium or indicated conditional media for 24 h. Gene expressions of *Il4*, *Vegfa*, and *Arg1* expressions in mouse naïve neutrophils were measured by the quantitative PCR analyses and compared to the levels in basal medium. Data are mean ± s.d.; $n = 3$ per group. *$P < 0.05$ between Basal and CM^{co} groups. C) The secretions of cytokines in conditioned media were measured by proteomic arrays. Selected cytokines are marked with colored outlines. D) Quantification of cytokine levels was carried out by densitometry. E) ECFC+MSC were cocultured in GelMA hydrogel and separated by magnetic-activated cell sorting (MACS) for gene expression analyses. ECFC or MSC monoculture served as controls. F) Quantitative PCR analyses of TGFβ1 expression in ECFCs sorted from ECFC+MSC coculture (labeled ECFC*) or from ECFC monoculture (ECFC). The same labeling applied to MSC (monoculture) and MSC* (sorted from coculture). DAPT was added to ECFC+MSC coculture to block Notch-mediated perivascular interaction. Data are mean ± s.d.; $n = 3$ per group; **$P <$ 0.01 between indicated groups.

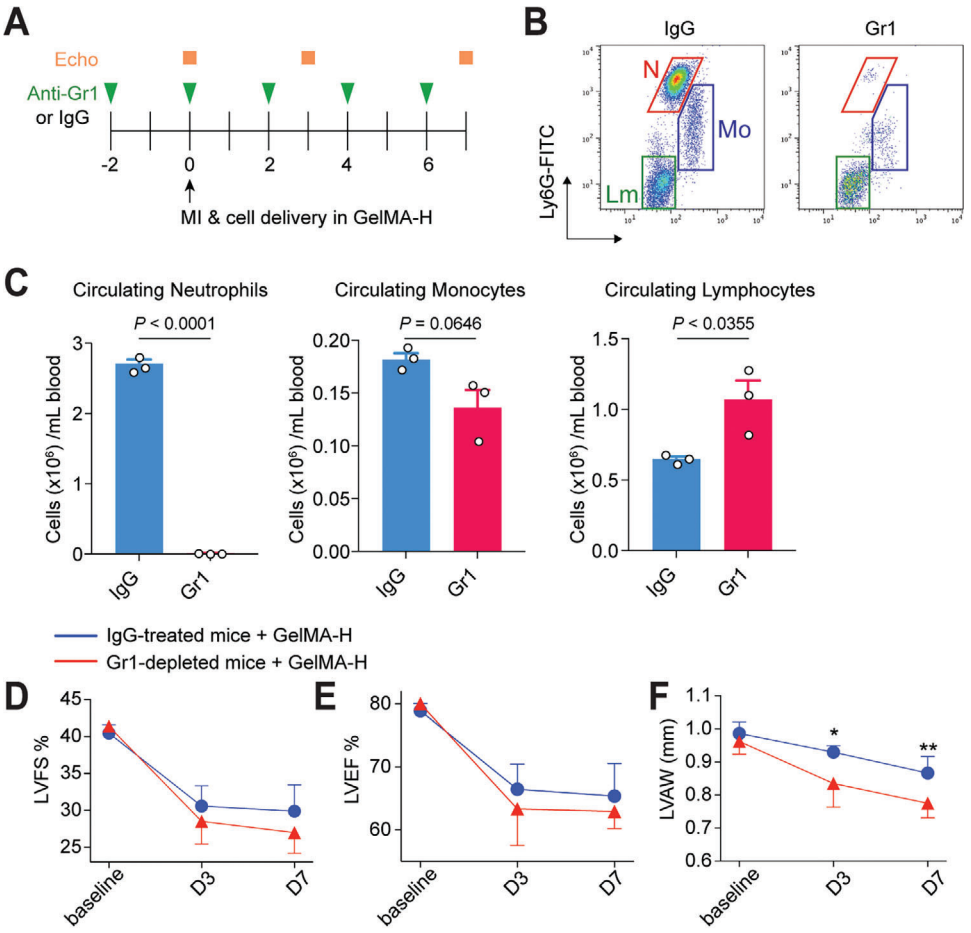

Figure 5. Neutrophil depletion abrogated the improvement in cardiac remodeling of human vascular cell delivery. A) Experimental schedule: anti-Gr-1 or IgG control antibody (200 μg each) was given via an intraperitoneal injection every 2 days. ECFC + MSC were delivered in GelMA-H into the ischemic myocardium at day 0. The effect of anti-Gr-1 depletion was monitored on days 3 and 7 post-MI by echocardiography. B) Representative flow cytometry analyses of circulating leukocytes from the blood of anti-Gr-1-treated or IgG-treated mice on day 2. N, neutrophils; Mo, monocytes; Lm, lymphocytes. C) Quantitative cytometric analyses of circulating leukocytes in the peripheral blood of anti-Gr-1-treated or IgG-treated mice. Data are mean ± s.d.; $n = 3$ per group; P values between IgG and Gr1 treatments are listed. D–F) Echocardiography analysis for cardiac function. Echocardiography was performed on anesthetized mice at days 3 and 7 post-MI following cell delivery in GelMA-H. Baseline data were obtained from mice within 1 h before performing LAD ligation. D) Left ventricular fractional shortening (LVFS). E) Left ventricular ejection fraction (LVEF). F) Left ventricular anterior wall thickness (LVAW). Data are mean ± s.d.; $n = 3$ for IgG-treated and $n = 4$ for Gr1-treated. $^*P < 0.1$, $^{**}P < 0.05$.

To gain a deeper understanding of the NR polarization factors, we performed a proteomic analysis of the conditioned media from the ECFCs + MSCs coculture (Figure 4C,D). Mixed conditioned media (a 1:1 mixture of CM^{ECFC} + CM^{MSC}; termed CM^{MIX}) obtained from separate ECFC and MSC monocultures served as a control. The secretion of several growth factors was induced in the ECFCs + MSCs coculture, including Activin A, IGFBP-1, Endoglin, Amphiregulin, and TGFβ1. The increase in TGF-β1 was consistent with our previous study that showed TGFβ1 promotes NR polarization.[45] We confirmed at the mRNA level that the ECFCs + MSCs coculture upregulated TGFβ1 expression only in ECFCs but not in MSCs (Figure 4E,F). Furthermore, exposing the ECFCs + MSCs coculture to the Notch inhibitor DAPT (a γ-secretase inhibitor) blocked the induction of TGFβ1 expression (Notch signaling is known to mediate vascular cell interaction[45]). Together, these results suggested that NR polarization was directly related to the engrafted human vascular progenitor cells in the infarcted tissues. Notch-mediated interaction of ECFCs and MSCs could modulate the early innate immune landscape by increasing TGFβ1 secretion by the ECFCs.

2.8. Neutrophil Depletion Abrogates the Improvement in Cardiac Remodeling

To confirm the critical role of host neutrophils during cardiac remodeling, we depleted circulating neutrophils in MI mice treated with GelMA-H. To achieve this, we treated mice from two days before LAD ligation to post-operative day 6 with either an anti-Gr1 or IgG (200 μg) control antibody given every 2 days via intraperitoneal injection (**Figure 5**A). This treatment with the anti-Gr1 antibody effectively depleted circulating neutrophils without altering blood monocytes and lymphocytes (Figure 5B,C). Importantly, neutrophil depletion nullified the

improvement in post-MI cardiac functions observed at days 3 and 7 in the GelMA-H group (LVEF and LVFS; Figure 5D,E) and significantly reduced myocardium thickness at day 7 (LVAW; Figure 5F). All three measurements of cardiac functions (LVEF, LVFS, and LVAW) in neutrophil-depleted mice were comparable to those observed in the untreated or GelMA-S groups (Figure 2). Collectively, these findings suggest that the depletion of neutrophils leads to excessive loss of myocardium, which could explain the progressive worsening of cardiac function. Indeed, host neutrophils were indispensable for the therapeutic effects exhibited by human vascular cells delivered in GelMA-H.

3. Discussion

Our study underscores the need for robust cell retention within the myocardium post-infarction to foster cardiac remodeling. We reveal that the use of photocrosslinked GelMA hydrogel notably amplifies the retention of human vascular progenitor cells in MI hearts, compared to its counterpart, the GelMA precursor solution. The effect of this enhanced retention is a marked improvement in post-MI remodeling, safeguarding cardiac function, and mitigating fibrosis. Importantly, we show that the administered ECFCs and MSCs establish a perfused vascular network within the infarcted myocardial region, fostering a pro-regenerative environment through the polarization of the recruited neutrophils, thus facilitating cardiac restoration.

Following myocardial infarction, the ischemic heart regions become a focal point for leukocyte infiltration, balancing precariously between instigating repair and exacerbating scarring and dysfunction.[15,61] The risk lies in the potential escalation to chronic inflammation, triggering adverse cardiac remodeling, and possible rupture due to an overabundance of innate immune cells.[62] Herein lies the paradox of neutrophils—they can facilitate repair post-MI, but also cause damage.[14,47] Delayed transition of post-MI neutrophils from a pro-inflammatory (NI) to a pro-regenerative (NR) phenotype can result in irreversible cardiac damage.[13,48,50,63,64] Yet, modulating this transition has been a challenge.

Our findings shed light on this issue, demonstrating that the transplantation of human vascular progenitor cells can expediently shift neutrophils toward the NR phenotype within two days post-MI. NR neutrophils are instrumental in tissue repair, as they temper pro-inflammatory reactions, promote M2 macrophage polarization, and stimulate angiogenesis, cell proliferation, and extracellular matrix remodeling.[45,48,49,56] Thus, we suggest that the strategic acceleration of an NR-driven regenerative response contributes to the therapeutic benefits of transplanting human vascular progenitor cells into infarcted hearts.

Mechanistically, TGFβ's capacity to direct neutrophils toward a pro-regenerative phenotype is well-established.[54,65] NRs form at injury sites via TGFβ-guided polarization of naïve neutrophils (N0) from bone marrow (BM).[65] Disrupting TGFβ signaling decreases NR subpopulations, impairing vascularization.[45] We previously demonstrated that human ECFCs and MSCs could form robust vascular networks in immunodeficient mice within a week[46,66,67] and that this process is contingent on host neutrophils expressing TGFβ receptor 2 (TGFBR2).[45] In neutrophil-depleted animals, vascularization was unachievable unless BM-derived neutrophils from unirradiated donors were adoptively transferred.[45] This emphasizes the pivotal role of TGFβ-TGFBR2 signaling in functional NR development.[45] Our current study strengthens the notion that engrafted human ECFCs are a pivotal source of NR-polarizing factors. We found that the medium from ECFC-MSC coculture in a GelMA hydrogel significantly enhances NR polarization, indicated by elevated NR signature genes, *Arg1*, *Vegfa*, and *Il4*, in mouse BM neutrophils. Importantly, ECFC-derived TGFβ1 up-regulation occurred exclusively in the presence of MSCs. When we impeded endothelial-perivascular cell interaction via Notch-signaling blockade, ECFCs failed to increase TGFβ1 expression. These findings underscore that delivering human vascular progenitor cells in GelMA hydrogel fosters TGFβ1 secretion and host NR engagement, shaping a pro-regenerative microenvironment for optimal post-MI cardiac healing.

The crosstalk between ECFCs and MSCs also led to an upregulation of additional cytokines, among which amphiregulin was the most notable. Nevertheless, we focused on the role of TGFβ1, which we previously established was the principal mediator of neutrophil polarization.[68] However, the potential roles of the other cytokines (Activin A, IGFBP-1, Endoglin, and Amphiregulin) should not be ignored. For example, Endoglin, an auxiliary receptor for TGFβ predominantly expressed on proliferating endothelial cells, along with Activin A, a member of the TGFβ superfamily that can also activate TGFβRs and downstream SMAD pathways,[69–71] may be involved in TGFβ-signaling mediated neutrophil polarization. Furthermore, Activin A, IGFBP-1, Endoglin, and Amphiregulin are known for their pro-angiogenic actions,[72–75] which suggests they may contribute to the therapeutic efficacy of GelMA-H. Thus, further research is warranted to elucidate the roles of these factors in NR polarization.

A major focus of our study is cell retention. Cell-based therapies for heart diseases present significant challenges. Systemic infusion, though direct, is both inefficient and potentially dangerous due to off-target cell accumulation, especially in the lungs.[76] Intracoronary injections, while targeted, carry the risk of cell-induced plug formation within capillaries en route to infarcted areas.[27,77] Intramyocardial injection, despite being precise and rapid, requires open-chest surgery for the epicardial approach, limiting its clinical use.[27] The endocardial approach, performed via a long catheter threaded into the left ventricle, circumvents this issue and thus offers higher translational potential.[78] However, regardless of the injection route, cell retention remains a shared hurdle, with the heart's "washout" effect expelling up to 80% of cells within hours of delivery.[28,79] Recognizing the crucial role of cell retention in cell-mediated cardiac repair,[27] the scientific focus has shifted toward bioengineering strategies to combat this issue, particularly through the development of novel biomaterials that improve cell retention, a critical step towards clinical translation.[7,80]

Various hydrogels have been investigated for cell delivery, including synthetic polymers and natural extracellular matrix (ECM) derivatives.[81–83] However, each has limitations: synthetic materials lack clear data on long-term biocompatibility, and natural ECMs gelate too slowly for optimal cell retention. To overcome these, we utilized GelMA, which can polymerize rapidly under UV illumination, ensuring cell retention and

offering an ideal biocompatible environment for cell engraftment and vascularization.[39,40] Also, GelMA is relatively inert, and its degradation yields non-toxic, non-immunogenic gelatin peptides, a natural ECM component.[38,39] Moreover, despite potential concerns about UV exposure, the UV spectrum (UVA–visible: 320–500 nm) used for GelMA crosslinking had minimal impact on human cells and mouse tissues.[40] Although visible light-responsive photoinitiators offer a UV alternative, they entail longer crosslinking times.[84] Indeed, we have previously confirmed the UV system's safety and practicality in minimally invasive heart delivery using a fiber-optic system with a catheter.[85]

Recent studies have investigated the use of additional materials such as metal nanoparticles (NPs), oligomers, and Polycaprolactone (PCL) for myocardial infarction treatment.[86–88] However, these materials come with their own set of challenges. For instance, metal NPs have raised concerns due to their low degradability, and oligomers have been known to induce toxicity. Additionally, understanding the full biological ramifications of PCL materials demands comprehensive research. On the other hand, our strategy employs an injectable cell-laden GelMA to deliver ECFCs and MSCs, which ensures enhanced cell viability and retention—offering a significant leap over some conventional techniques. Moreover, our methodology fosters host regenerative neutrophil involvement, which plays a pivotal role in repairing myocardial infarction.

Beyond cell retention, a recent study showed that acellular GelMA hydrogel could improve post-MI survival rates and ventricular function by providing mechanical support.[89] However, our study used a much softer GelMA hydrogel (≈2 kPa elastin modulus), which we previously showed is necessary to enable the viability of the encapsulated human ECFCs and MSCs.[39] Indeed, our late time point histological analyses (2–4 weeks) revealed no observable GelMA-H bulk gel, suggesting its degradation in the mouse hearts. This complete degradation is consistent with our previous findings that 1M ᴍ GelMA (i.e., 49.8% ᴍ methacrylation degree) degrades rapidly in vivo due to matrix metallopeptidase (MMP)-mediated cleavage of the gelatin backbone.[39] Consequently, our GelMA-cell injection does not provide the same mechanical support as the stiffer GelMA patch used by Ptaszek et al.,[89] and the improvement in heart function we observed was attributed to high cell retention rather than GelMA's mechanical stability.

Our study had several limitations. Foremost was the use of immunodeficient mice to enable human cell transplantation. Although their myeloid cell lineage is intact, their compromised B and T cell immunity could influence outcomes. This concern is accentuated by the increased susceptibility to bacterial infections during long-term neutrophil depletion observed in such mice.

A significant operational constraint was the 7-day experimental endpoint, chosen for two primary reasons. First, our previous observations indicated that the most pronounced difference in MI recovery between successful and non-successful treatments occurred on day 7. Second, we limited the study duration to minimize the animals' burden in alignment with ethical guidelines. While a more extended period of neutrophil depletion might have revealed greater differences between treatment groups, the potential for confounding effects due to heightened infection risks was a serious consideration.

Other limitations stem from the mouse MI model's constraints. We induced MI by permanent ligation of the LAD artery in mouse hearts. However, a cardiac I, which is more clinically relevant, would have been preferable but is challenging to implement consistently in small mouse hearts. Similarly, mimicking the probable clinical route for intramyocardial cell delivery through a minimally invasive catheter procedure is extremely difficult in mice and rats.

Another important consideration is the photo-crosslinking depth. Given that the human myocardium is substantially thicker than that of mice, the successful photocrosslinking of GelMA hydrogel, particularly in a clinical setting, can pose a significant challenge. Nonetheless, the field of hydrogel crosslinking has seen remarkable advancements, leading to the development of hydrogels with increased crosslinking depths.[90] Various techniques have contributed to this progress. For example, selecting appropriate photoinitiators—such as Rose Bengal, a photosensitizer that effectively absorbs light at a wavelength of 530 nm, which collagen readily absorbs[91]—can enhance the photoinitiator's activation at greater hydrogel depths.

Increasing light intensities and extending exposure times are other strategies to attain deeper crosslinking depths.[90,92] Yet, it is essential to finely tune these parameters to prevent potential damage to the hydrogel and the cells within. Specific light wavelengths can also offer better penetration through thick tissues; notably, two-photon lasers emit light at double the energy of the photons absorbed by the photoinitiator, allowing deeper hydrogel activation.[93]

In addition to these techniques, other factors like the molecular weight of the polymer, concentration of the crosslinking agent, and the crosslinking reaction temperature can significantly influence the crosslinking depth of GelMA hydrogels.[92] By optimizing these parameters, it is feasible to achieve increased crosslinking depth within the hydrogel. We envision that leveraging these advancements in our GelMA-H-based treatment modality could effectively surmount the challenges presented by the thickness of the human heart, thereby paving the way for successful clinical application. Nevertheless, given the complexities of controlling photocrosslinking, it is premature to put forward the optimal conditions. Our study represents a crucial step forward, but a comprehensive investigation is needed to determine the optimal condition that balances cell retention, light penetration, and blood vessel formation. Such investigation would ideally be conducted in a large animal model to simulate the clinical setting more closely.

In the clinics, proper management of the photo-crosslinking depth will be essential, as even injections at the microscale can influence therapeutic outcomes. UV-A, which can reach the dermis layer (>1 mm), has the potential for deeper myocardial penetration. This deep penetration could enhance treatment efficacy for MI patients, who often exhibit reduced LV wall thickness. However, care must be taken when injecting beyond 1 mm to avoid myocardial puncture due to heart movement.

Last, the evaluation of cardiac functions in mice was limited to imaging-based measurements for live animals and histological examination for end-point experiments. Future investigations with larger animals might offer more detailed analyses, including invasive hemodynamics with pressure-volume loops for long-term evaluations.

4. Conclusion

We have developed an innovative cell delivery method for treating myocardial infarction. Our approach involves the intramyocardial injection of vascular progenitor cells suspended in a GelMA precursor solution, followed by transmyocardial UV illumination, forming an in situ photocrosslinked hydrogel that effectively retains the cells within ischemic myocardial tissue. This method ensures high viability and cell retention, offering a significant advantage over liquid or unmodified ECM gel injections. The enhanced cell retention allowed us to investigate the therapeutic impact of human vascular progenitor cells post-MI. Our findings revealed that engrafted cells facilitated beneficial myocardial remodeling and stabilization of cardiac functions post-MI through engagement and polarization of host pro-regenerative neutrophils via TGFβ signaling. This proof-of-concept study paves the way for further research, including large animal testing, incorporation of catheter-mediated injectate and UV light delivery systems, and exploration of additional cell types, such as iPSC-derived cardiomyocytes. We believe our research holds promise for developing an off-the-shelf cell-based therapy with the potential to treat acute myocardial infarction effectively.

5. Experimental Section

Cell Culture: Human ECFCs and MSCs were isolated under institutional review board-approved protocols from human umbilical cord blood and subcutaneous adipose tissue, respectively, as previously described.[43,94] ECFCs were cultured on 1% (w/v) gelatin-coated plates and maintained in ECFC-medium: EGM-2 (except for hydrocortisone; PromoCell) supplemented with 20% FBS (Hyclone) and 1× glutamine-penicillin-streptomycin (GPS; Invitrogen). ECFCs express CD31, VE-cadherin, von Willebrand factor (vWF), but not CD90, CD45, or CD14. MSCs were cultured on uncoated plates using mesenchymal stem cell growth medium (MSCGM; ATCC) with MSC growth supplement (ATCC) and 1× GPS. MSCs express CD90 and PDGFRβ, but not endothelial or hematopoietic markers. ECFCs and MSCs between passages 6 and 12 were used for all the experiments.

Synthesis of GelMA: The synthesis of GelMA was carried out as per the procedure outlined in a previous work by the authors.[39] This involved dissolving porcine skin gelatin in phosphate-buffered saline, reacting it with methacrylic anhydride, dialyzing to remove unreacted methacrylic anhydride, and lyophilizing the product. The degree of methacrylation, quantified by an NMR spectrometer (Varian INOVA), was found to be consistent with the previous results (i.e., 49.8% functionalization to original amino groups).[39]

Preparation of GelMA Precursor Solution: A GelMA precursor solution was prepared by dissolving lyophilized GelMA (5 w/v% final) and photoinitiator Irgacure 2959 (0.5 w/v%) in PBS at 80 °C and then cooled to 37 °C in a water bath. Human ECFCs and MSCs (5×10^5 cells for each cell type) were resuspended in 100 µL of GelMA precursor solution. The cell/GelMA mixture was kept at 37 °C, protected from light, and used within 1 h.

Mouse Model of Myocardial Infarction and Intramyocardial Cell Delivery: The myocardial infarction mouse model and subsequent cell delivery was conducted following the approved protocol by the Institutional Animal Care and Use Committee at Boston Children's Hospital, using male NOD.SCID mice (NOD.Cg-Prkdcscid/J; 10–12 weeks, 30–35 g; Jackson Laboratory). The mice were anesthetized and intubated, followed by controlled ventilation. A left thoracotomy exposed the anterior surface of the heart, where myocardial infarction was induced by the permanent ligation of the left anterior descending (LAD) artery, verified by a color change in the left ventricular wall. Subsequently, the cell/GelMA mixture was injected into the myocardium and UV photocrosslinked using an OmniCure S2000 UV lamp and adjusted with a UV intensity meter (G&R Labs) to achieve in situ polymerization of cell-laden GelMA hydrogel. Uniform illumination was maintained through a consistent distance between the light guide and the mouse myocardium. Post-procedure, the thorax was closed, air was withdrawn, and the mice were extubated and returned to their cages after spontaneous breathing recovery.

Quantification of Cell Retention by In Vivo Bioluminescence Imaging: Luciferase-expressing ECFCs (luc-ECFCs) were generated via transfection using a PiggyBac vector carrying a CMV promoter-driven firefly luciferase reporter gene and a super PiggyBac transposase expression vector (System Biosciences), following a previously described protocol.[95] A 5:1 ratio between transposon and transposase vectors and 2.4 µg of DNA per 1×10^6 ECFCs was used. Following puromycin selection, stable expression of the luciferase reporter gene in ECFCs was achieved. These luc-ECFCs were then mixed with non-labeled MSCs (ratio 1:1; total 1×10^6 cells) and suspended in 100 µL of GelMA precursor solution. This cell suspension was injected into the infarcted myocardium and subjected to UV illumination (GelMA-H group). Cell injection without UV illumination (GelMA-S group) was performed as a control. Bioluminescence imaging of the mice was done at 3, 24, 48, and 72 h post-cell injection, using an IVIS 200 Imaging System (Xenogen Corporation). After being anesthetized and administered with luciferin (125 mg kg^{-1} body weight), bioluminescence was measured 5 min post-luciferin administration. Data analysis was conducted with Live Image 3.0 (Xenogen Corporation). The bioluminescence measurement obtained 15 min post-injection of the same cell suspension into arrested mouse hearts was used as the baseline for this study.

Echocardiographic Measurement: Cardiac function following LAD ligation and treatments were evaluated by using a high-frequency ultrasound system Vevo 2100 (VisualSonics) with a 30 MHz central frequency scan head. To facilitate the echocardiography, the mice were anesthetized with isoflurane and placed on a heated pad in the left lateral decubitus position. 2D echocardiography and M-mode images were obtained using a short axis view from the mid-LV at the tips of the papillary muscles. The left ventricular ejection fraction (LVEF) and left ventricular fractional shortening (LVFS) were calculated from LV dimensions in the 2D short axis view. Echocardiography was performed on each mouse 1 h before LAD ligation to obtain a reference of baseline cardiac function. Cardiac function was monitored post-MI at 3 days and 1, 2, and 4 weeks.

Histology and Immunofluorescence Staining: Hearts were harvested and processed at defined time points post-treatment. After weighing, they were fixed overnight in 10% neutral-buffered formalin and subsequently embedded in paraffin. 7 µm thick sections were then prepared through the infarcted area. Hematoxylin-eosin or Masson's trichrome staining was performed on these sections, and myocardial wall thickness and fibrosis were quantified using ImageJ software (version 1.44, NIH). For immunostainings, the procedure initiated with deparaffinization and rehydration of the sections, followed by antigen retrieval performed at 95 °C for 30 min in Tris-EDTA buffer. Blocking was then done for 30 min with 5% blocking serum, and the sections were incubated with primary antibodies overnight at 4 °C. Human-specific vimentin antibody (clone V9; Abcam) and Ulex Europaeus Agglutinin I (UEA-I; Vector Laboratories) was used to stain human blood vessels.[95] The sections were then exposed to fluorescent secondary antibodies for 1 h at room temperature and nuclei counterstained with DAPI, before mounting with a fluorescent mounting medium (Dako). To quantify human vascularization in the myocardial infarction region, staining was done for human-specific UEA-1 and high-resolution images of the entire infarcted area in each tissue section were captured. Human microvessel density was determined by counting the number of vessels in these images and calculating the average density (vessels per mm^2).

Flow Cytometry: Mouse hearts were harvested from euthanized mice, rinsed in cool PBS to remove blood, and enzymatically digested with collagenase A (1 mg mL^{-1}; Roche Life Science) and dispase (2.5 U mL^{-1}; BD Biosciences) for 2 h at 37 °C. The retrieved cells were incubated with PerCP-conjugated anti-mouse CD45 (1:100; BD Biosciences), FITC-conjugated mouse Ly6G (1:100; clone 1A8, Biolegend), PE-conjugated anti-mouse F4/80 (1:100; eBiosciences), APC-conjugated anti-mouse CD206 (1:50; Biolegend), and APC.Cy7-conjugated anti-mouse CXCR2 (1:50; Biolegend) antibodies. Flow cytometric analyses were performed using a BD LSRFortess flow cytometer (BD Biosciences) and FlowJo

software (Tree Star Inc.). Murine hematopoietic cells were identified as mCD45$^+$ cells. Ly6G$^+$F4/80$^-$ and Ly6G$^-$F4/80$^+$ mouse hematopoietic cells were neutrophils or monocytes/macrophages, respectively. Within Ly6G$^+$F4/80$^-$ neutrophils, neutrophil subpopulations were classified into naïve neutrophils (N0; CXCR2$^-$), pro-inflammatory neutrophils (NI; CXCR2$^+$CD206$^-$), and pro-regenerative neutrophils (NR; CXCR2$^+$CD206$^+$).

To determine human ECFC and MSC retention, the retrieved cells were stained with PerCP-conjugated anti-mouse CD45, FITC-conjugated anti-human CD31 (1:50 Biolegend), and PE-conjugated anti-human CD90 (1:100 Biolegend). ECFCs were identified as mCD45$^-$hCD31$^+$hCD90$^-$ cells and MSCs were mCD45$^-$hCD31$^-$hCD90$^+$.

RNA-Sequencing (RNAseq) Analysis: RNAseq was conducted on infarcted myocardial tissues and uninjured controls (three biological replicates per group). RNA was extracted using an RNeasy Mini Kit and quality assessed with an Agilent Bioanalyzer. Libraries were prepared and sequenced by GENEWIZ. Data quality was checked with FastQC, reads were aligned to the UCSC mm10 genome using STAR aligner,[96] and checked using Qualimap.[97] Transcript expressions were quantified against the Ensembl release GRCm38 transcriptome annotation using Salmon, with data imported into R for gene level aggregation with tximport. Differential expression was identified with DESeq2,[98] using Wald significance test for pairwise comparison, adjusting *P*-values with Benjamini–Hochberg procedure. Genes with an adjusted *P*-value < 0.05 and absolute log2 fold change > 1 were considered differentially expressed. PCA analysis was performed on normalized, variance-stabilized reads. LRT was used for all sample comparison. Functional enrichment of differentially expressed genes was determined with Fisher's exact test via the cluster Profiler package. Heat maps, volcano plots, and other visualizations were generated with pheatmap and ggplot2 packages.

Quantitative Real-Time PCR Analysis: Total RNA was extracted from cells using the RNeasy Mini Kit (Qiagen) following the manufacturer's workflow. RNA concentration was measured by the NanoDrop 8000 spectrophotometer (Thermo Fisher), and RNA purity was evaluated by the ratio of absorbance at 260 and 280 nm. The cDNA synthesis was processed by High-Capacity RNA-to-cDNA Kit (Thermo Fisher). The quantitative real-time PCRs were performed on the QuantStudio 6 Flex Feal-Time PCR System with PowerUp SYBM Green Master Mix (Thermo Fisher). GAPDH served as the housekeeping gene. Sequences of primers for real-time PCR are listed in Table S1, Supporting Information.

ECFC-MSC Coculture and Conditioned Medium Generation: Samples of conditioned medium were collected from GelMA hydrogels containing ECFC + MSC coculture (1:1 ratio; total 5×10^5 cells per 100 µL gel) or monoculture (only ECFC or MSC alone; total 5×10^5 cells per 100 µL gel) over 8 days in vitro. To this end, cell-laden GelMA hydrogels were cultured in 3 mL tubes with 500 µL of Basal medium (EBM-2, 5% FBS medium) refreshed every 24 h. Collected samples of conditioned medium were filtered (0.2 µm) and then concentrated tenfold (Amicon Ultra centrifugal filters; 3 kDa cut off; Millipore).

To determine the effect of ECFC-MSC coculture on TGFβ1 expression, cells were retrieved from GelMA hydrogels after in vitro coculture for 8 days by enzymatical digestion (collagenase/dispase; 1 h at 37 °C). ECFCs were sorted out from MSCs by MACS using magnetic beads (Dynabeads; Thermo Fisher Scientific) coated with anti-human CD31 antibodies. The purity of MACS-sorted cells was validated by the cell-type specific mRNA expressions of human *CD31* or *PDGFRβ* for ECFCs or MSCs, respectively, by the quantitative real-time PCR analysis. Retrieved cells from gels containing only ECFC or MSC alone served as controls. For notch-signaling inhibition studies, GelMA hydrogel containing ECFC + MSC coculture were treated with the γ-secretase inhibitor DATP (10 µM in EGM-2 with 5% FBS; Selleckchem) for 24 h before harvesting conditioned media.[45]

Human Cytokine Protein Array: The presence of selected cytokines was evaluated in samples of conditioned medium with Proteome profiler human angiogenesis array (R&D Systems) according to the manufacturer's instructions. Antigen-antibody reactions were visualized using LumiGLO substrate (Kirkegaard & Perry Laboratories, Inc.) and chemiluminescent sensitive film (Kodak). Densitometry was performed by image analysis (ImageJ) to estimate the amount of protein present in each sample.

Isolation of Mouse Bone Marrow Neutrophils: Mouse femur bone was dissected from euthanized mice and cut at both ends. A 23G needle was used for flushing the bone marrow out with ice-cold HBSS buffer. After RBC lysis, mouse bone marrow neutrophils were sorted from the bone marrow cell suspension using a mouse neutrophil isolation kit that enriches for CD11b$^+$Ly6G$^+$ cells (Miltenyi Biotec; negative selection using a cocktail that contains anti-CD5, -CD45R, -CD49b, -CD117, -F4/80, and -Ter119 antibodies). Isolated neutrophils were maintained in StemSpan H3000 medium (STEMCELL Technologies) supplemented with GlutaMAX (1X; Thermo Fisher Scientific), ExCyte (0.2%; Merck Millipore), Am580 retinoic acid agonist (2.5 mM; Sigma-Aldrich) and human G-CSF (150 ng mL^{-1}; PeproTech).

In Vitro Neutrophil Polarization Assay: Due to the limited lifespan of neutrophils, the freshly isolated mouse bone marrow neutrophils were used immediately for conditioned medium studies. Mouse bone marrow neutrophils (5×10^6 cells) were cultured for 24 h in 1 mL of StemSpan H3000 medium supplemented with tenfold concentrated conditioned media (reconstituted in 9:1 volume ratio). Basal medium (EBM-2, 5% FBS medium) served as a control. After 24 h, neutrophils were collected for quantitative PCR analysis of NR polarization markers (*Il4, Vegfa*, and *Arg1*). Mouse neutrophils treated with recombinant human TGFβ1 (10 ng mL^{-1}; PeproTech) for 24 h served as a positive control for NR polarization.[54]

Neutrophil Depletion: For neutrophil depletion studies, either anti-mouse Ly-6G/Ly-6C Gr1 (Bio X Cell) or control (IgG_{2b}; Bio X Cell) antibodies were administered intraperitoneally into mice every 2 days from 2 days before LAD ligation to post-operative day 6. Anti-Gr1 given at 200 µg per mouse was shown to be sufficient to deplete neutrophils in the circulation, confirmed by flow cytometry using FITC-conjugated Ly6G antibody (1:100; clone 1A8, Biolegend).[44] The authors' group and others have previously substantiated the validity of this neutrophil depletion model.[68,99–101]

Microscopy: Images were taken by the Axio Observer Z1 inverted microscope (Carl Zeiss) and AxioVision Rel. 4.8 software. Fluorescent images were taken with an ApoTome.2 Optical sectioning system (Carl Zeiss) and 20× or 40× objective lens. Non-fluorescent images were taken with an AxioCam MRc5 camera using a 10× or 20× objective lens.

Statistical Analyses: All statistical analyses were performed using the GraphPad Prism v.7 software (GraphPad Software Inc.). The sample size, including the number of mice per group, was chosen to ensure adequate power and based on historical laboratory data. No exclusion criteria were applied for all analyses. All data were expressed as mean ± standard deviation of the mean (s.d.). Comparisons between multiple groups were performed by ANOVA followed by Bonferroni's post-test analysis. Unpaired two-tailed Student's *t*-test was used for comparisons between two groups. A value of $P < 0.05$ was considered to be statistically significant.

Supporting Information

Supporting Information is available from the Wiley Online Library or from the author.

Acknowledgements

This work was supported by grants from the National Institutes of Health (R01HL128452, R01HL152133, and R01AR080086 to J.M.M.-M.).

Conflict of Interest

The authors declare no conflict of interest.

Author Contributions

X.H., J.M.M.-M., and R.-Z.L. conceived and designed the project. X.H., A.C.L., I.D., N.O., G.-B.I., and R.-Z.L. performed the experimental work. All authors discussed and analyzed the data and edited the results. X.H., R.-Z.L., and J.M.M.-M. wrote the manuscript.

Data Availability Statement

The data that support the findings of this study are available from the corresponding author upon reasonable request.

Keywords

cell delivery, gelatin methacryloyl, myocardial infarction, pro-regenerative neutrophil

Received: May 16, 2023
Revised: August 8, 2023
Published online:

[1] G. W. Reed, J. E. Rossi, C. P. Cannon, *Lancet* **2017**, *389*, 197.
[2] V. L. Roger, A. S. Go, D. M. Lloyd-Jones, E. J. Benjamin, J. D. Berry, W. B. Borden, D. M. Bravata, S. Dai, E. S. Ford, C. S Fox, H. J. Fullerton, C. Gillespie, S. M. Hailpern, J. A. Heit, V. J. Howard, B. M. Kissela, S. J. Kittner, D. T. Lackland, J. H. Lichtman, L. D. Lisabeth, D. M. Makuc, G. M. Marcus, A. Marelli, D. B. Matchar, C. S. Moy, D. Mozaffarian, M. E. Mussolino, G. Nichol, N. P. Paynter, E. Z. Soliman, et al., *Circulation* **2012**, *125*, e2.
[3] P. C. Westman, M. J. Lipinski, D. Luger, R. Waksman, R. O. Bonow, E. Wu, S. E. Epstein, *J. Am. Coll. Cardiol.* **2016**, *67*, 2050.
[4] J. Tamargo, J. López-Sendón, *Nat. Rev. Drug Discov.* **2011**, *10*, 536.
[5] G. W. Stone, C. L. Grines, D. A. Cox, E. Garcia, J. E. Tcheng, J. J. Griffin, G. Guagliumi, T. Stuckey, M. Turco, J. D. Carroll, B. D. Rutherford, A. J. Lansky, *N. Engl. J. Med.* **2002**, *346*, 957.
[6] G. Montalescot, P. Barragan, O. Wittenberg, P. Ecollan, S. Elhadad, P. Villain, J.-M. Boulenc, M.-C. Morice, L. Maillard, M. Pansiéri, R. Choussat, P. Pinton, *N. Engl. J. Med.* **2001**, *344*, 1895.
[7] C. Huang, Z. Zhang, Q. Guo, L.i Zhang, F. Fan, Y.u Qin, H. Wang, S. Zhou, W. Ou-Yang, H. Sun, X. Leng, X. Pan, D. Kong, L. Zhang, D. Zhu, *Adv. Healthcare Mater.* **2019**, *8*, 1900840.
[8] R. Katarzyna, *Curr. Cardiol. Rev.* **2017**, *13*, 223.
[9] N. Dib, H. Khawaja, S. Varner, M. Mccarthy, A. Campbell, *J. Cardiovasc. Transl. Res.* **2011**, *4*, 177.
[10] N. Pavo, S. Charwat, N. Nyolczas, A. Jakab, Z. Murlasits, J. Bergler-Klein, M. Nikfardjam, I. Benedek, T. Benedek, I. J. Pavo, B. J. Gersh, K. Huber, G. Maurer, M. Gyöngyösi, *J. Mol. Cell. Cardiol.* **2014**, *75*, 12.
[11] S. Popescu, M. B. Preda, C. I. Marinescu, M. Simionescu, A. Burlacu, *Int. J. Mol. Sci.* **2021**, *22*, 5631.
[12] R. J. Vagnozzi, M. Maillet, M. A. Sargent, H. Khalil, A. K. Z. Johansen, J. A. Schwanekamp, A. J. York, V. Huang, M. Nahrendorf, S. Sadayappan, J. D. Molkentin, *Nature* **2020**, *577*, 405.
[13] I. Andreadou, H. A. Cabrera-Fuentes, Y. Devaux, N. G. Frangogiannis, S. Frantz, T. Guzik, E. A. Liehn, C. P. C. Gomes, R. Schulz, D. J. Hausenloy, *Cardiovasc. Res.* **2019**, *115*, 1117.
[14] L. F. Trajano, N. Smart, *npj Regener. Med.* **2021**, *6*, 8.
[15] L. Fang, X.-L. Moore, A. M. Dart, L.-M. Wang, *J Geriatr. Cardiol.* **2015**, *12*, 305.
[16] N. J. Pluijmert, D. E. Atsma, P. H. A. Quax, *Front. Cardiovasc. Med.* **2021**, *8*, 647785.
[17] X. Mei, K.e Cheng, *Front. Cardiovasc. Med.* **2020**, *7*, 610364.
[18] S. Dimmeler, J. Burchfield, A. M. Zeiher, *Arterioscler. Thromb.* **2008**, *28*, 208.
[19] Z.-A. Zhao, X. Han, W. Lei, J. Li, Z. Yang, J. Wu, M. Yao, X.-A. Lu, L. He, Y. Chen, B. Zhou, S. Hu, *Circ. Res.* **2018**, *123*, e21.
[20] S. Fukushima, A. Varela-Carver, S. R. Coppen, K. Yamahara, L. E. Felkin, J. Lee, P. J. R. Barton, C. M. N. Terracciano, M. H. Yacoub, K. Suzuki, *Circulation* **2007**, *115*, 2254.
[21] D. Sürder, R. Manka, V. L. Cicero, T. Moccetti, K. Rufibach, S. Soncin, L. Turchetto, M. Radrizzani, G. Astori, J. Schwitter, P. Erne, M. Zuber, C. Auf der Maur, P. Jamshidi, O. Gaemperli, S. Windecker, A. Moschovitis, A. Wahl, I. Bühler, C. Wyss, S. Kozerke, U. Landmesser, T. F Lüscher, R. Corti, *Circulation* **2013**, *127*, 1968.
[22] P. E. Szmitko, P. W. M. Fedak, R. D. Weisel, D. J. Stewart, M. J. B. Kutryk, S. Verma, *Circulation* **2003**, *107*, 3093.
[23] M. Gnecchi, H. He, O. D. Liang, L. G. Melo, F. Morello, H. Mu, N. Noiseux, L. Zhang, R. E. Pratt, J. S. Ingwall, V. J. Dzau, *Nat. Med.* **2005**, *11*, 367.
[24] K.-T. Kang, M. Coggins, C. Xiao, A. Rosenzweig, J. Bischoff, *Angiogenesis* **2013**, *16*, 773.
[25] S.-J. Park, R.i Y. Kim, B.-W. Park, S. Lee, S. W. Choi, J.-H. Park, J. J. Choi, S.-W. Kim, J. Jang, D.-W. Cho, H.-M. Chung, S.-H. Moon, K. Ban, H.-J. Park, *Nat. Commun.* **2019**, *10*, 3123.
[26] X. Hong, N. Oh, K. Wang, J. Neumeyer, C. N. Lee, R.-Z. Lin, B. Piekarski, S. Emani, A. K. Greene, I. Friehs, P. J. Del Nido, J. M. Melero-Martin, *Angiogenesis* **2021**, *24*, 327.
[27] J. Li, S. Hu, D. Zhu, K. Huang, X. Mei, B. L. de, J. Abad, K. Cheng, *J. Am. Heart Assoc.* **2021**, *10*, e020402.
[28] C. J. Teng, J. Luo, R. C. J. Chiu, D. Shum-Tim, *J. Thorac. Cardiovasc. Surg.* **2006**, *132*, 628.
[29] J. Terrovitis, R. Lautamäki, M. Bonios, J. Fox, J. M. Engles, J. Yu, M. K. Leppo, M. G. Pomper, R. L. Wahl, J. Seidel, B. M. Tsui, F. M. Bengel, M. R. Abraham, E. Marbán, *J. Am. Coll. Cardiol.* **2009**, *54*, 1619.
[30] Z. Liu, R. Mikrani, H. M. Zubair, A. Taleb, M. Naveed, M. M. F. A. Baig, Q. Zhang, C. Li, M. Habib, X. Cui, K. R. Sembatya, H. Lei, X. Zhou, *Eur. J. Pharmacol.* **2020**, *876*, 173049.
[31] P. Menasché, *Nat. Rev. Cardiol.* **2018**, *15*, 659.
[32] V. Crisostomo, C. Baez, J. L. Abad, B. Sanchez, V. Alvarez, R. Rosado, G. Gómez-Mauricio, O. Gheysens, V. Blanco-Blazquez, R. Blazquez, J. L. Torán, J. G. Casado, S. Aguilar, S. Janssens, F. M. Sánchez-Margallo, L. Rodriguez-Borlado, A. Bernad, I. Palacios, *Stem Cell Res Ther* **2019**, *10*, 152.
[33] B. Vrtovec, G. Poglajen, L. Lezaic, M. Sever, D. Domanovic, P. Cernelc, A. Socan, S. Schrepfer, G. Torre-Amione, F. Haddad, J. C. Wu, *Circ. Res.* **2013**, *112*, 165.
[34] J. R. Garcia, P. F. Campbell, G. Kumar, J. J. Langberg, L. Cesar, L. Wang, A. J. García, R. D. Levit, *JACC Basic Transl. Sci.* **2017**, *2*, 601.
[35] X. Cui, J. Tang, Y. Hartanto, J. Zhang, J. Bi, S. Dai, S. Z. Qiao, K.e Cheng, H.u Zhang, *ACS Appl. Mater. Interfaces* **2018**, *10*, 37783.
[36] Y. Ichihara, M. Kaneko, K. Yamahara, M. Koulouroudias, N. Sato, R. Uppal, K. Yamazaki, S. Saito, K. Suzuki, *Biomaterials* **2018**, *154*, 12.
[37] J. Tang, X. Cui, T. G. Caranasos, M. T. Hensley, A. C. Vandergriff, Y. Hartanto, D. Shen, H.u Zhang, J. Zhang, K.e Cheng, *ACS Nano* **2017**, *11*, 9738.
[38] J. W. Nichol, S. T. Koshy, H. Bae, C. M. Hwang, S. Yamanlar, A. Khademhosseini, *Biomaterials* **2010**, *31*, 5536.
[39] Y.-C. Chen, R.-Z. Lin, H. Qi, Y. Yang, H. Bae, J. M. Melero-Martin, A. Khademhosseini, *Adv. Funct. Mater.* **2012**, *22*, 2027.
[40] R.-Z. Lin, Y.-C. Chen, R. Moreno-Luna, A. Khademhosseini, J. M. Melero-Martin, *Biomaterials* **2013**, *34*, 6785.
[41] K. Yue, G. Trujillo-De Santiago, M. M. Alvarez, A. Tamayol, N. Annabi, A. Khademhosseini, *Biomaterials* **2015**, *73*, 254.
[42] T. E. Robey, M. K. Saiget, H. Reinecke, C. E. Murry, *J. Mol. Cell. Cardiol.* **2008**, *45*, 567.
[43] J. M. Melero-Martin, Z. A. Khan, A. Picard, X. Wu, S. Paruchuri, J. Bischoff, *Blood* **2007**, *109*, 4761.
[44] K.-T. Kang, R.-Z. Lin, D. Kuppermann, J. M. Melero-Martin, J. Bischoff, *Stem Cells Int.* **2017**, *7*, 770.
[45] R.-Z. Lin, C. N. Lee, R. Moreno-Luna, J. Neumeyer, B. Piekarski, P. Zhou, M. A. Moses, M. Sachdev, W. T. Pu, S. Emani, J. M. Melero-Martin, *Nat. Biomed. Eng.* **2017**, *1*, 0081.
[46] R.-Z. Lin, R. Moreno-Luna, D. Li, S.-C. Jaminet, A. K. Greene, J. M. Melero-Martin, *Proc. Natl. Acad. Sci. USA* **2014**, *111*, 10137.

[47] C. Silvestre-Roig, Q. Braster, A. Ortega-Gomez, O. Soehnlein, *Nat. Rev. Cardiol.* **2020**, *17*, 327.
[48] M. Horckmans, L. Ring, J. Duchene, D. Santovito, M. J. Schloss, M. Drechsler, C. Weber, O. Soehnlein, S. Steffens, *Eur. Heart J.* **2017**, *38*, 187.
[49] W. Yang, Y. Tao, Y. Wu, X. Zhao, W. Ye, D. Zhao, L. Fu, C. Tian, J. Yang, F. He, L.i Tang, *Nat. Commun.* **2019**, *10*, 1076.
[50] Y. Ma, A. Yabluchanskiy, R. P. Iyer, P. L. Cannon, E. R. Flynn, M. Jung, J. Henry, C. A. Cates, K. Y. Deleon-Pennell, M. L. Lindsey, *Cardiovasc. Res.* **2016**, *110*, 51.
[51] R. E. Von Leden, K. N. Parker, A. A. Bates, L. J. Noble-Haeusslein, M. H. Donovan, *Exp. Neurol.* **2019**, *317*, 144.
[52] E. Kolaczkowska, P. Kubes, *Nat. Rev. Immunol.* **2013**, *13*, 159.
[53] J. Blázquez-Prieto, I. López-Alonso, C. Huidobro, G. M. Albaiceta, *Am. J. Respir. Cell Mol. Biol.* **2018**, *59*, 289.
[54] M. Ohms, S. Möller, T. Laskay, *Front. Immunol.* **2020**, *11*, 532.
[55] R. Voskuhl, *Nat. Immunol.* **2020**, *21*, 1477.
[56] A. R. Sas, K. S. Carbajal, A. D. Jerome, R. Menon, C. Yoon, A. L. Kalinski, R. J. Giger, B. M. Segal, *Nat. Immunol.* **2020**, *21*, 1496.
[57] Y. Hou, D. Yang, R. Xiang, H. Wang, X. Wang, H. Zhang, P. Wang, Z. Zhang, X. Che, Y. Liu, Y. Gao, X. Yu, X. Gao, W. Zhang, J. Yang, C. Wu, *Int. Immunopharmacol.* **2019**, *77*, 105970.
[58] M. Peiseler, P. Kubes, *J. Clin. Invest.* **2019**, *129*, 2629.
[59] B. Cai, D. Lin, Y. Li, L.e Wang, J. Xie, T. Dai, F. Liu, M. Tang, L. Tian, Y. Yuan, L. Kong, S. G. F. Shen, *Adv. Sci.* **2021**, *8*, 2100584.
[60] J. Wang, *Cell Tissue Res.* **2018**, *371*, 531.
[61] S. A. Dick, S. Epelman, *Circ. Res.* **2016**, *119*, 159.
[62] N. G. Frangogiannis, *J. Cardiovasc.Pharmacol.* **2014**, *63*, 185.
[63] E. Vafadarnejad, G. Rizzo, L. Krampert, P. Arampatzi, A.-P. Arias-Loza, Y. Nazzal, A. Rizakou, T. Knochenhauer, S. R. Bandi, V. A. Nugroho, D. J. J. Schulz, M. Roesch, P. Alayrac, J. Vilar, J.-S. Silvestre, A. Zernecke, A.-E. Saliba, C. Cochain, *Circ. Res.* **2020**, *127*, e232.
[64] D. M. Calcagno, C. Zhang, A. Toomu, K. Huang, V. K. Ninh, S. Miyamoto, A. D. Aguirre, Z. Fu, J. Heller Brown, K. R. King, *J. Am. Heart Assoc.* **2021**, *10*, e019019.
[65] Z. G. Fridlender, J. Sun, S. Kim, V. Kapoor, G. Cheng, L. Ling, G. S. Worthen, S. M. Albelda, *Cancer Cell* **2009**, *16*, 183.
[66] R.-Z. Lin, J. M. Melero-Martin, *Methods* **2012**, *56*, 440.
[67] J. M. Melero-Martin, M. E. De Obaldia, S.-Y. Kang, Z. A. Khan, L. Yuan, P. Oettgen, J. Bischoff, *Circ. Res.* **2008**, *103*, 194.
[68] R.-Z. Lin, C. N. Lee, R. Moreno-Luna, J. Neumeyer, B. Piekarski, P. Zhou, M. A. Moses, M. Sachdev, W. T. Pu, S. Emani, J. M. Melero-Martin, *Nat. Biomed. Eng.* **2017**, *1*, 0081.
[69] J. Massagué, *Nat. Rev. Mol. Cell Biol.* **2012**, *13*, 616.
[70] E. Rossi, C. Bernabeu, D. M. Smadja, *Front. Med.* **2019**, *6*, 10.
[71] M. M. Matzuk, T. R. Kumar, A. Vassalli, J. R. Bickenbach, D. R. Roop, R. Jaenisch, A. Bradley, *Nature* **1995**, *374*, 354.
[72] D. M. W. Zaiss, W. C. Gause, L. C. Osborne, D. Artis, *Immunity* **2015**, *42*, 216.
[73] T. Slater, N. J. Haywood, C. Matthews, H. Cheema, S. B. Wheatcroft, *Cytokine Growth Factor Rev.* **2019**, *46*, 28.
[74] P. Ten Dijke, M.-J. Goumans, E. Pardali, *Angiogenesis* **2008**, *11*, 79.
[75] C. Ervolino De Oliveira, M. Dourado, Í. Sawazaki-Calone, M. Costa De Medeiros, C. Rossa Júnior, N. De Karla Cervigne, J. Esquiche León, D. Lambert, T. Salo, E. Graner, R. Coletta, *Int. J. Oncol.* **2020**, *57*, 364.
[76] R. Zhao, Z. Su, J. Wu, H.-L. Ji, *Oncotarget* **2017**, *8*, 30511.
[77] A. A. L. Kindi, *Front. Biosci.* **2008**, *13*, 2421.
[78] W. Sherman, T. P. Martens, J. F. Viles-Gonzalez, T. Siminiak, *Nat. Clin. Pract. Cardiovasc. Med.* **2006**, *3*, S57.
[79] F. van den Akker, D. A. M. Feyen, P. van den Hoogen, L. W. van Laake, E. C. M. van Eeuwijk, I. Hoefer, G. Pasterkamp, S. A. J. Chamuleau, P. F. Grundeman, P. A. Doevendans, J. P. G. Sluijter, *Eur. Heart J.* **2017**, *38*, 184.
[80] Z. Li, S. Hu, K.e Cheng, *Acc. Chem. Res.* **2019**, *52*, 1687.
[81] J. Tang, X. Cui, T. G. Caranasos, M. T. Hensley, A. C. Vandergriff, Y. Hartanto, D. Shen, H.u Zhang, J. Zhang, K.e Cheng, *ACS Nano* **2017**, *11*, 9738.
[82] X. Cui, J. Tang, Y. Hartanto, J. Zhang, J. Bi, S. Dai, S. Z. Qiao, K.e Cheng, H.u Zhang, *ACS Appl. Mater. Interfaces* **2018**, *10*, 37783.
[83] Y. Ichihara, M. Kaneko, K. Yamahara, M. Koulouroudias, N. Sato, R. Uppal, K. Yamazaki, S. Saito, K. Suzuki, *Biomaterials* **2018**, *154*, 12.
[84] S. Sharifi, H. Sharifi, A. Akbari, J. Chodosh, *Stem Cells Int.* **2021**, *11*, 23276.
[85] E. T. Roche, A. Fabozzo, Y. Lee, P. Polygerinos, I. Friehs, L. Schuster, W. Whyte, A. M. Casar Berazaluce, A. Bueno, N. Lang, M. J. N. Pereira, E. Feins, S. Wasserman, E. D. O'cearbhaill, N. V. Vasilyev, D. J. Mooney, J. M. Karp, P. J. Del Nido, C. J. Walsh, *Sci. Transl. Med.* **2015**, *7*, 306ra149.
[86] Y. Wang, Z. Fan, Q.i Li, J. Lu, X. Wang, J. Zhang, Z. Wu, *J. Mater. Chem. B* **2023**, *11*, 4980.
[87] Z. Wu, W. Li, S. Cheng, J. Liu, S. Wang, *Nanomed.: Nanotechnol. Biol. Med.* **2023**, *47*, 102616.
[88] W. Liang, J. Chen, L. Li, M. Li, X. Wei, B. Tan, Y. Shang, G. Fan, W. Wang, W. Liu, *ACS Appl. Mater. Interfaces* **2019**, *11*, 14619.
[89] L. M. Ptaszek, R. Portillo Lara, E. Shirzaei Sani, C. Xiao, J. Roh, X. Yu, P. A. Ledesma, C. Hsiang Yu, N. Annabi, J. N. Ruskin, *J. Am. Heart Assoc.* **2020**, *9*, e014199.
[90] C. D. O'Connell, B. Zhang, C. Onofrillo, S. Duchi, R. Blanchard, A. Quigley, J. Bourke, S. Gambhir, R. Kapsa, C. D. Bella, P. Choong, G. G. Wallace, *Soft Matter* **2018**, *14*, 2142.
[91] S. Eckes, J. Braun, J. S. Wack, U. Ritz, D. Nickel, K. Schmitz, *Int. J. Mol. Sci.* **2020**, *21*, 7408.
[92] J. He, Y. Sun, Q. Gao, C. He, K.e Yao, T. Wang, M. Xie, K. Yu, J. Nie, Y. Chen, Y. He, *Adv. Healthcare Mater.* **2023**, https://doi.org/10.1002/adhm.202300395.
[93] M. Lunzer, L. Shi, O. G. Andriotis, P. Gruber, M. Markovic, P. J. Thurner, D. Ossipov, R. Liska, A. Ovsianikov, *Angew. Chem., Int. Ed.* **2018**, *57*, 15122.
[94] R.-Z. Lin, R. Moreno-Luna, R. Muñoz-Hernandez, D. Li, S.-C. S. Jaminet, A. K. Greene, J. M. Melero-Martin, *Angiogenesis* **2013**, *16*, 735.
[95] K. Wang, R.-Z. Lin, X. Hong, A. H. Ng, C. N. Lee, J. Neumeyer, G. Wang, X.i Wang, M. Ma, W. T. Pu, G. M. Church, J. M. Melero-Martin, *Sci. Adv.* **2020**, *6*, eaba7606.
[96] A. Dobin, C. A. Davis, F. Schlesinger, J. Drenkow, C. Zaleski, S. Jha, P. Batut, M. Chaisson, T. R. Gingeras, *Bioinformatics* **2013**, *29*, 15.
[97] F. García-Alcalde, K. Okonechnikov, J. Carbonell, L. M. Cruz, S. Götz, S. Tarazona, J. Dopazo, T. F. Meyer, A. Conesa, *Bioinformatics* **2012**, *28*, 2678.
[98] M. I. Love, W. Huber, S. Anders, *Genome Biol.* **2014**, *15*, 550.
[99] J. Stackowicz, F. Jönsson, L. L. Reber, *Front. Immunol* **2020**, *10*, 3130.
[100] K. W. Bruhn, K. Dekitani, T. B. Nielsen, P. Pantapalangkoor, B. Spellberg, *Results Immunol.* **2016**, *6*, 5.
[101] J. M. Daley, A. A. Thomay, M. D. Connolly, J. S. Reichner, J. E. Albina, *J. Leukocyte Biol.* **2008**, *83*, 64.